CellPress

Chemistry & Biology
Article

Crystal Structure of a PCP/Sfp Complex Reveals the Structural Basis for Carrier Protein Posttranslational Modification

Peter Tufar,[1,2] Simin Rahighi,[2,3,6] Femke I. Kraas,[4] Donata K. Kirchner,[1] Frank Löhr,[1] Erik Henrich,[1] Jürgen Köpke,[5] Ivan Dikic,[2,3] Peter Güntert,[1] Mohamed A. Marahiel,[4] and Volker Dötsch[1,2,*]

[1]Institute of Biophysical Chemistry and Center for Biomolecular Magnetic Resonance, Goethe University Frankfurt/Main, Max-von-Laue-Strasse 9, 60438 Frankfurt, Germany

[2]Buchmann Institute for Molecular Life Sciences, Goethe University Frankfurt/Main, Max-von-Laue-Strasse 15, 60438 Frankfurt, Germany

[3]Institute of Biochemistry II, Goethe University Medical School, Theodor-Stern-Kai 7, 60590 Frankfurt, Germany

[4]Department of Chemistry, Biochemistry, Philipps University Marburg, Hans-Meerwein-Strasse, 35032 Marburg, Germany

[5]Max Planck Institute of Biophysics, Department of Molecular Membrane Biology, Max-von-Laue-Strasse 3, 60438 Frankfurt, Germany

[6]Present address: Department of Structural Biology, Stanford University School of Medicine, Stanford, CA 94305-5126, USA

*Correspondence: vdoetsch@em.uni-frankfurt.de

http://dx.doi.org/10.1016/j.chembiol.2014.02.014

SUMMARY

Phosphopantetheine transferases represent a class of enzymes found throughout all forms of life. From a structural point of view, they are subdivided into three groups, with transferases from group II being the most widespread. They are required for the post-translational modification of carrier proteins involved in diverse metabolic pathways. We determined the crystal structure of the group II phosphopantetheine transferase Sfp from *Bacillus* in complex with a substrate carrier protein in the presence of coenzyme A and magnesium, and observed two protein-protein interaction sites. Mutational analysis showed that only the hydrophobic contacts between the carrier protein's second helix and the C-terminal domain of Sfp are essential for their productive interaction. Comparison with a similar structure of a complex of human proteins suggests that the mode of interaction is highly conserved in all domains of life.

INTRODUCTION

Carrier-protein-driven synthesis of primary and secondary metabolites is an essential process in every organism (Crosby and Crump, 2012). Among these carrier proteins, the acyl carrier protein or domain (ACP) of fatty acid synthase (FAS) is conserved throughout all kingdoms of life (Chan and Vogel, 2010). Its fold with a four-helix bundle as the structural core (Figure 1A) is found not only in FAS but also in many other biosynthetic pathways, ranging from peptidyl carrier proteins (PCPs) in nonribosomal peptide synthetases (NRPSs) (Condurso and Bruner, 2012; Hur et al., 2012) and ACPs in polyketide synthases (PKSs) (Keatinge-Clay, 2012), which are mainly present in bacteria and fungi, to carrier proteins that shuttle intermediates for metabolism of lysine in yeast (Ehmann et al., 1999) and humans (Praphanphoj et al., 2001). The posttranslational conversion of carrier proteins into their holo form is a prerequisite for their function. This is accomplished by phosphopantetheinylation of the hydroxyl group of a conserved serine side chain located at the N terminus of the second helix. A conformational equilibrium has been described for TycC3_PCP, the third PCP domain of the tyrocidine A synthetase subunit C from *Bacillus brevis* (Koglin et al., 2006). Besides the common four-helix bundle structure referred to as the A/H state, a second conformer exists for the apo-PCP lacking the 4′-phosphopantetheine (ppan) cofactor. In this so-called A state, the third helix is disordered and all other helices are shortened, resulting in a partly unfolded and therefore more flexible structure.

All phosphopantetheine transferases (PPTs) (Beld et al., 2014), which catalyze the transfer of the cofactor derived from coenzyme A (CoA) (Figure 1C) onto a carrier protein, share a fundamental domain that comprises a central, three-stranded, antiparallel β sheet with a $\beta_1/\beta_3/\beta_2$ topology and a stretch of ~80 amino acids inserted between the first two β strands. This stretch adopts a mainly helical fold located on one side of the β sheet, whereas the other side acts as an oligomerization interface (Figure 1B). The formation of oligomers is essential for the function of the PPT, as the active site with the binding pocket for CoA and the carrier protein is formed by the interface of two monomers.

Structurally, three different groups of PPTs can be distinguished. Holo acyl carrier protein synthases (AcpSs) represent the first group (Elovson and Vagelos, 1968). Consisting of an intermolecular trimer of single PPT domains (Parris et al., 2000), they are found in most bacteria as the modifying enzyme for the ACP of FAS. The PPTs of group III are mainly found in fungi, where the FAS is composed of multidomain peptide chains containing a PPT domain (Fichtlscherer et al., 2000). In the active megasynthase, these PPT domains are located on the outside as separated, nonfunctional monomers that are incapable of interacting with the ACP domain (Lomakin et al., 2007). Investigations of the excised PPT domain of the FAS from yeast showed that it forms catalytic trimers analogous to group I PPTs, and it was proposed that this situation occurs during the assembly of the active FAS enzyme complex (Johansson et al., 2009).

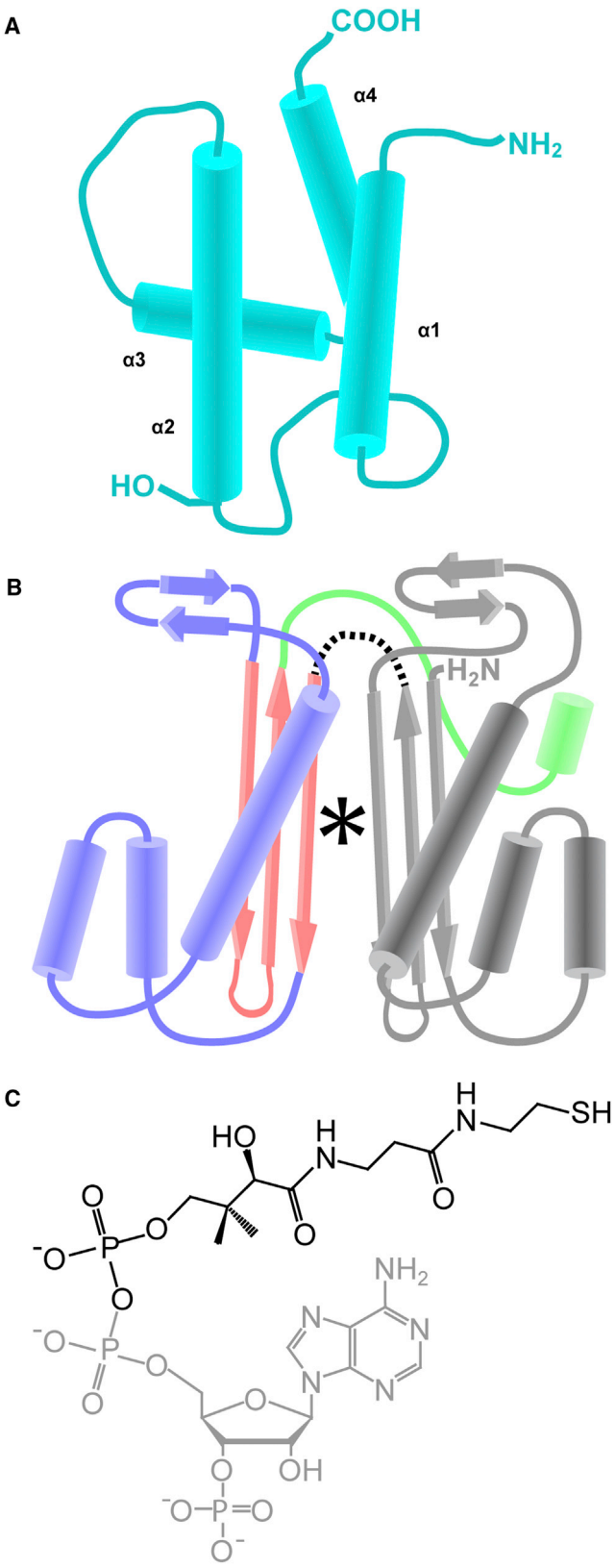

Figure 1. The Key Elements of Phosphopantetheinylation

(A) Carrier proteins consist of four helices, with the conserved serine located at the N terminus of the second helix.

(B) In type II PPTs, an N-terminal PPT domain (gray) and a C-terminal PPT domain (colored) are connected by a short linker (dashed line). Each PPT domain consists of a central β sheet (red) with a mainly helical insert (purple) between the first two strands. The C terminus of the protein forms an extended region (green) that embraces the N-terminal PPT domain. The two PPT domains interact via their central β sheets, thus forming the binding pocket for CoA and the interface for the interaction with the carrier protein (asterisk).

(C) During the reaction, the ppan moiety (black) of CoA is transferred onto the carrier protein with 3′,5′-adenosine bisphosphate (gray) as a side product.

In contrast to the two other types, PPTs from group II harbor two fused PPT domains within one protein (Lambalot et al., 1996). Thus, they do not oligomerize in an intermolecular fashion, but act as single proteins that can be seen as intramolecular pseudo-dimers (Reuter et al., 1999). In microorganisms, PPTs of group II are involved in secondary metabolism, and it has been shown that they are capable of modifying the ACPs of primary metabolism in vitro (Lambalot et al., 1996). Their high tolerance with respect to carrier proteins accepted as a substrate may explain why the sole human PPT is a member of this group (Praphanphoj et al., 2001).

Sfp, which is required for cofactor loading on the surfactin NRPS in *Bacillus subtilis*, is a structurally and functionally well-characterized group II PPT. It exhibits a broad promiscuity toward CoA derivatives and carrier proteins. Hence, it is frequently used in biotechnological approaches to load carrier proteins with ppan conjugated with molecules such as amino acids (Belshaw et al., 1999), peptides (Sieber et al., 2003), fatty acids (Kosa et al., 2012), and fluorescent labels (La Clair et al., 2004).

In the present work, we solved the crystal structure of Sfp, CoA, and the active-site alanine mutant of TycC3_PCP, which form a stable ternary complex, at 2.0 Å resolution. Furthermore, we solved the structure of TycC3_PCP(S45A) by using liquid-state NMR techniques, and the results show that, in contrast to what we proposed in our previous work (Koglin et al., 2006), the free active-site mutant PCP is in the A/H state conformation in solution. Based on the structure of the complex, we identified several motifs involved in the protein-protein interaction. We investigated the impact of the residues involved on the velocity of the transfer reaction and the stability of the complex by performing a ppan transfer assay and isothermal titration calorimetry (ITC). Remarkably, the key interactions for formation of the carrier protein/PPT complex seem to be conserved in group II PPTs from bacteria to humans (Bunkoczi et al., 2007).

RESULTS

Structure of Sfp in Complex with TycC3_PCP(S45A)

An active-site serine-to-alanine mutant of the carrier protein TycC3_PCP(S45A) was chosen for crystallization in order to prevent the ppan transfer reaction but still facilitate the formation of the complex in the presence of CoA. We crystallized the heterodimeric protein complex consisting of Sfp and TycC3_PCP(S45A) sandwiching CoA, and solved its structure to a resolution of 2.0 Å (Figure 2A).

Sfp within the complex consists of two structurally similar PPT domains (M1-D100 and I104-A206; root-mean-square deviation

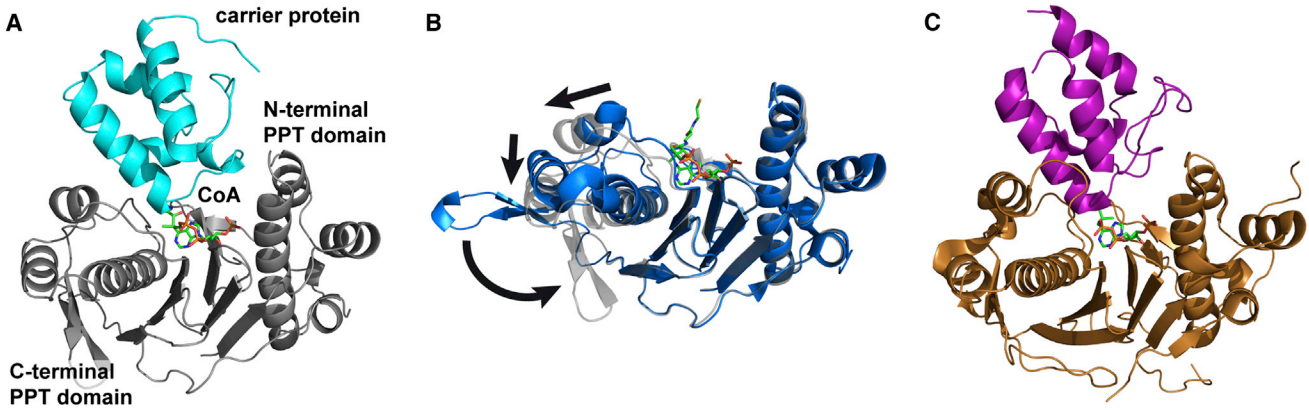

Figure 2. Structure of the TycC3_PCP(S45A)/Sfp Complex

(A) PCP (cyan) and Sfp (gray) form a complex with CoA (sticks) buried in their interface.

(B) Major differences between free Sfp (blue, PDB 1QR0) and its complex with PCP (semitransparent gray; PCP not shown) are a relocation of the first helix in the C-terminal PPT domain that widens the binding pocket for PCP and a reorientation of β1′/β2′of the C-terminal PPT domain (movements with respect to the location in the structure of free Sfp are indicated by arrows).

(C) The structure of the human ACP/PPT complex (PDB 2CG5) shows a high similarity to the PCP/Sfp complex, although parts of the carrier proteins differ in their orientation.

See also Table S2.

[rmsd] ~3.1 Å over 94 C^{α} pairs), each spanning ~100 residues, and a C-terminal extension (A207-L224). Both domains form the expected central antiparallel β sheet with a β1/β3/β2 arrangement. β1 and β2 are linked by an ~80 amino acid insert containing three α helices (α1, α2, and α3) and an antiparallel β sheet (β1′/β2′). Helix α3 is situated diagonally across the central β sheet. While α1 and α2 cover the N-terminal half of α3, the C-terminal half interacts with β1′/β2′. The elongated C terminus of Sfp passes around β1 and α3 of the N-terminal PPT domain and ends as a short helix located between β1, α1, and α3 of the N-terminal PPT domain.

The structure of Sfp within the PCP/Sfp complex resembles the known type II PPT structure. Compared with the structures of Sfp in complex with CoA (Reuter et al., 1999) (Protein data Bank [PDB] 1QR0; Figure 2B) and the human PPT in complex with CoA and the ACP domain of FAS (Bunkoczi et al., 2007) (PDB 2CG5; Figure 2C), it shows an rmsd of ~1.5 Å and ~2.0 Å over 207 and 221 C^{α} pairs, respectively. The most prominent differences in comparison with the known Sfp structure are the reorientation of α1/α2 (K110-Q139) and the loop containing β1′/β2′ (G158-S187) in the C-terminal PPT domain. The movement of α1/α2 increases their distance to the N-terminal domain by 4–5 Å, resulting in a larger cavity for PCP binding. The ~90° flip of the loop harboring β1′/β2′ is more severe. Although in both structures the loop is in close proximity to α2, α3, and β2 of Sfp's second PPT domain, these extended hydrophobic and polar contacts are formed in the crystal structure of free Sfp by intermolecular contacts and in the structure of the PCP/Sfp complex in an intramolecular manner.

Cofactor Binding by Sfp

The binding of CoA's base and sugar, as well as the 3′ phosphate group by Sfp, does not differ between the structures in the presence and absence of PCP. A Mg ion that is coordinated by CoA and residues of β1 and α3 of the C-terminal PPT domain is essential for the transfer reaction. The coordination of this Mg ion changes between the free Sfp and the PCP/Sfp complex (Figures 3A and 3B). In the structure without PCP, the Mg ion is coordinated by side-chain carboxyl groups from D107, E109, and E151 of Sfp, CoA's pyrophosphate, and a water molecule. In the structure of the complex, the carboxyl group of E151 is rotated by ~90°, facilitating a 0.6 Å shift of the Mg ion toward the oxygen of the 5′ α phosphate accompanied by a slight reorientation of the β phosphate and the water molecule. As a result, the Mg ion is almost perfectly coordinated in five out of six octahedral positions by D107, E151, CoA's pyrophosphate, and a water molecule. Due to the larger distance, E109 can no longer occupy the sixth position; instead, a second water molecule is clearly visible in the electron density map at this position. The position of this water might be further stabilized by a hydrogen bond to the indole amine of W147. This arrangement is similar to the one observed in the human PPT with CoA (Bunkoczi et al., 2007) (PDB 2C43), although the position of the second water molecule is more disordered in that structure (Figure 3C). Another feature of the PCP/Sfp structure is the presence of a second Mg ion in the active site. It is coordinated by CoA's 5′ α phosphate, the carbonyl and side chain of Sfp's H90, and three water molecules. The electron density that we identified as this second Mg ion was observed in the structures of Sfp and the human PPT as well, but was assigned as water molecules (Figures 3D–3F).

In contrast to previous structures, the whole pantetheine moiety of CoA shows electron density, whereas a discrete positioning of this part of the cofactor was not observed in the structure of Sfp in complex with CoA or in the human PPT/ACP complex. The oxygen atoms of its two amide bonds point toward Sfp's L161/S162, and the terminal thiol group is located between Sfp's E72/Y73 and helix 3 of the PCP (Figure S1 available online). Since multiple examples have shown that Sfp is very tolerant toward modifications of CoA's thiol group, ranging from a

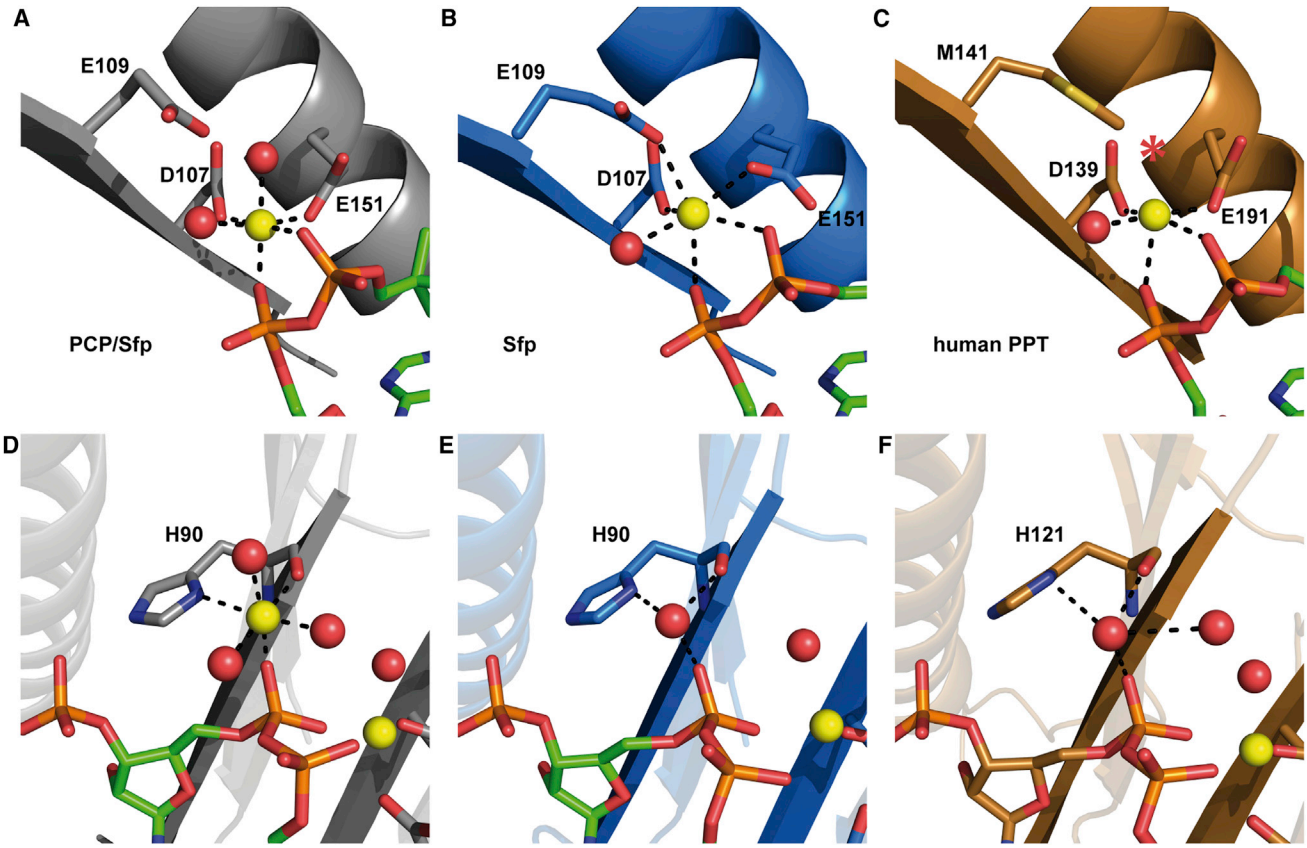

Figure 3. Coordination of the Magnesium Ions

(A–C) The coordination of the catalytic Mg ion (yellow ball) differs between Sfp's complex with PCP (A) and the free Sfp (B). The former resembles the situation in the human PPT (C; PDB 2C43), but in this structure one water molecule (asterisk) shows only weak electron density and is sterically hindered by the side chain of M141.

(D–F) In the structure of the PCP/Sfp complex, a second Mg ion is present and is coordinated by H90 of Sfp, CoA, and three water molecules (D). In the other structures, electron density is observed in the same position, but is assigned as a water molecule even though it is similarly coordinated by histidine and CoA (E and F).

See also Figures S1 and S2.

substitution with an amino group (Liu and Bruner, 2007; Worthington and Burkart, 2006) to attachment of amino acids, peptides, and fatty acids, it is likely that the location of the pantetheine moiety in solution is more disordered within the gap between Sfp and the carrier protein than the crystal structure suggests.

PCP Is Not in the A State

The PCP in complex with Sfp and CoA shows electron density for its whole helical core, whereas short parts of the N and C termini (P2-Q7 and S85-H91) are not resolved. According to mass-spectrometric analysis, M1 is cleaved in vivo (data not shown). The secondary structure and fold of PCP indicate clearly that it is in the regular carrier protein conformation (A/H state) and not in the A state as we proposed previously (Koglin et al., 2006). To determine which conformation TycC3_PCP(S45A) adopts in solution, we solved its structure by NMR spectroscopy. Contrary to the previous prediction, the PCP (Figure 4) has the same overall fold as observed in the crystallized complex (rmsd 0.70 Å).

Interaction between Sfp and PCP

Based on the crystal structure, two interaction sites between PCP and Sfp were detected. The amide hydrogen of Y36 in Sfp's N-terminal domain and the backbone carbonyl oxygen of PCP's Q40 form an intermolecular hydrogen bond (Figure 5B). The second, more expanded interaction site comprises nonpolar contacts between the C-terminal domain of Sfp and the second helix of PCP. Sfp's hydrophobic patch is formed by side chains located in the first helix and the preceding loop (I114, I118, F122, and F123), and the third helix and the succeeding loop (F143, Y144, W147, L161, and L165) in the C-terminal domain, respectively. These side chains point toward the binding pocket between the two PPT domains and form a small cavity. This cavity is occupied by the side chains of L46 and M49 of PCP's second helix (Figures 5C and 5D). Sequence alignments show that these two positions are always occupied with hydrophobic residues in carrier proteins that are natural targets of group II PPTs, and that hydrophobic residues, which probably form the binding interface for these carrier proteins, are present in diverse group II PPTs (Figure 5E). In addition, a glycine positioned three

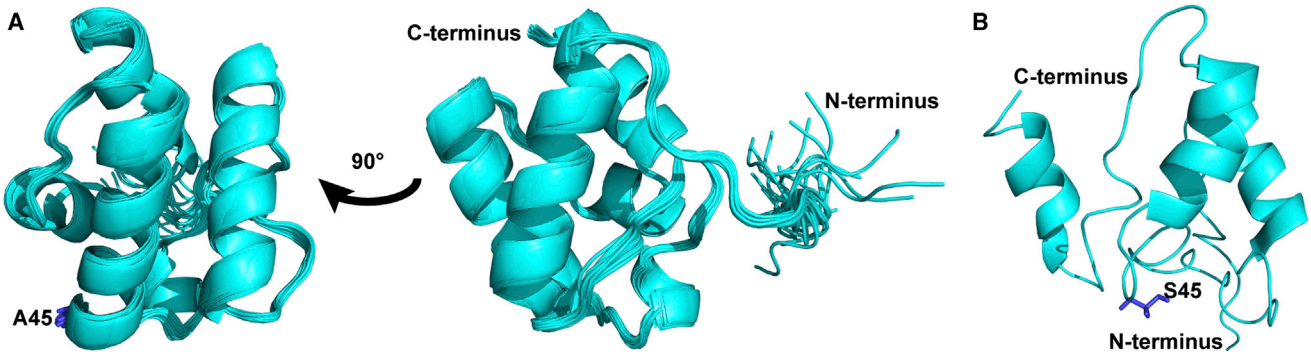

Figure 4. NMR Investigations on TycC3_PCP(S45A)

The 20 lowest-energy NMR structures of the PCP mutant (A; H86-91 omitted) show that the mutant PCP is not in the A state conformation (B; PDB 2GDY) as was previously proposed.

See also Table S3.

residues N terminal to the active-site serine occurs in most carrier proteins. In the structure of the complex, this residue (G42) has a positive ϕ angle. Thus, it seems to be necessary for a correct orientation of the hydrogen bond and the hydrophobic patches (Figure 5A).

Mutational Analysis of the PCP-Sfp Interaction

To investigate the proposed importance of these amino acids for the protein-protein interaction, mutants of both proteins were created. Sfp(Y36P) was generated to destroy the intermolecular hydrogen bond. In the wild-type (WT) and active-site mutant, PCP mutations L46A, L46N, L46D or M49D were introduced to disrupt the hydrophobic interaction, and G42A was introduced to hinder the correct orientation of the two interaction sites. Although the G42A mutation abolished the expression in vivo, the expression in vitro resulted in a protein pellet that could be refolded after it was dissolved in urea.

All mutant proteins exhibited the same monomeric properties as the WT proteins when studied by size-exclusion chromatography (data not shown), and their correct fold and sufficient stability were confirmed by circular dichroism spectroscopy (Figure S3). Changes in the binding of CoA to Sfp(Y36P) were ruled out by results showing that this mutant had approximately the same affinity for CoA as Sfp(WT) (Table 1) in an ITC experiment. Furthermore, in vivo and cell-free expressed TycC3_PCP(S45A) showed similar binding affinities to Sfp(WT) at 5°C with dissociation constants (K_D) of 0.74 and 0.94 μM, respectively, whereas the WT carrier protein expressed in vivo and in vitro behaved virtually identically in the ppan transfer assay (Figure S4A).

To probe the effect of the mutations on the stability of the PCP/Sfp complex, the PCP mutants harboring the S45A mutation and WT and mutant Sfp were investigated by ITC. In the presence of CoA, almost all PCP variants could be titrated with Sfp(WT) at 5°C and 25°C; only TycC3_PCP(G42A,S45A) was not stable at the higher temperature. At both temperatures, TycC3_PCP (S45A) showed comparable K_D values of 0.74 μM at 5°C and 0.92 μM at 25°C. TycC3_PCP(G42A,S45A) was the only double mutant with a detectable but significantly higher K_D (39.7 μM), and the K_D for all other mutants was too high to be determined by ITC. Titration of Sfp(Y36P) with TycC3_PCP (S45A) showed no binding at 25°C, but at 5°C a K_D of 54.3 μM could be determined (Table 1).

To compare the stability of the complex with the velocity of the phosphopantetheinylation reaction, apo-PCPs with an intact active-site serine were incubated with Sfp(WT) in the presence of CoA. The formation of holo-PCPs at different time points was quantitatively monitored by liquid chromatography/mass spectrometry analysis and revealed a dependency of the reaction's velocity on the mutation in the PCP (Figure 6). The L46A mutation reduced the reaction speed compared with TycC3_PCP(WT), whereas the effect of the L46N mutation was more severe, and TycC3_PCP(L46D) showed hardly any product formation even after incubation for 1 hr. Introduction of an aspartate at position 49 had a less drastic effect, and holo-TycC3_PCP(M49D) was produced considerably faster than holo-TycC3_PCP(L46N). Unexpectedly, the fastest turnover was observed for the reactions of TycC3_PCP(G42A) with Sfp(WT), and for WT PCP incubated with Sfp(Y36P). On the other hand, the modification of TycC3_PCP(L46N) was significantly slower when Sfp(WT) was substituted with Sfp(Y36P) (Figure S4B).

DISCUSSION

In previous investigations (Koglin et al., 2006), we showed that PCP domains, in both the apo and holo forms, can adopt different conformations and that these conformations exchange dynamically with each other. For apo-TycC3_PCP in solution, double peaks were observed in different NMR spectra. These two sets of peaks represent the A state and the A/H state conformation, the structures of which we calculated based on nuclear Overhauser effect (NOE) signals (Koglin et al., 2006). In the same study, we observed that mutation of the active-site serine of the PCP to alanine led to the disappearance of one set of peaks, and we suggested, based on chemical-shift data, that the mutated PCP is locked in the less well-structured A state conformation. Furthermore, we proposed a docking model of the PCP/Sfp complex with the PCP in the A state conformation (Koglin et al., 2006). However, the structures of isolated TycC3_PCP

(S45A) (as determined by NMR) and TycC3_PCP(S45A) in complex with Sfp (as determined by X-ray crystallography), both reported here, now reveal that this mutant adopts the A/H state conformation. In the docking model, this arrangement was not possible because the PCP in the A/H state conformation did not fit into the binding pocket of the Sfp structure determined by Reuter et al. (1999) that was used for modeling. Here, we show that the binding pocket of Sfp opens by ~5 Å, so the PCP in the A/H state conformation can bind (Figure 2B). There is no evidence that the A state conformation is involved in the PCP-Sfp interaction. However, the only known functional interaction of an apo-PCP is its phosphopantetheinylation by a PPT. Therefore, the biological function and relevance of the A state conformation observed for the WT apo-TycC3_PCP are unknown and require further investigation.

The intermolecular contacts in the structure of Sfp in complex with CoA were previously referred to as an artifact of crystallization (Reuter et al., 1999). However, the reorientation of β1′/β2′ and α1/α2 indicate a flexibility of this region that might be related to regulation of the enzyme's activity. Yet, from this region only α1 is involved in the formation of the binding interface for PCP, and the binding pocket for CoA seems to be unaffected by the rearrangement. Since the PCP in the A/H state conformation does not fit in the narrow binding pocket of Sfp observed in the structure of the CoA complex, the relevance of this alternative conformation remains unclear. Furthermore, no similar rearrangement has been observed in the corresponding structures of the human PPT (Bunkoczi et al., 2007).

The crystal structure presented here is a PPT/carrier protein complex in the presence of CoA with a well-resolved active site including the essential cation and its inner coordination sphere, and thus provides insights into the catalysis of the ppan transfer reaction. Three mechanisms for the deprotonation of the side chain of S45 have been proposed. Based on the structure of Sfp, direct complexation and activation by the Mg ion (Reuter et al., 1999) was suggested, whereas mutational studies on Sfp (Mofid et al., 2004) and human PPT (Bunkoczi et al., 2007) suggested deprotonation by the conserved glutamate side chain (E151 and E191, respectively). For the *Bacillus* AcpS, deprotonation by an activated water molecule was proposed (Parris et al., 2000).

For our structure, we mutated the active-site serine of PCP in order to suppress the reaction in favor of the formation of a stable complex; however, it can also be modeled in silico. Modeling of the hydroxyl group in the (−)-gauche conformation brings it into close proximity to the catalytic center, whereas in the two other rotamers it is pointing away from the catalytic center. In this situation, a direct interaction of the hydroxyl group with the Mg ion seems unlikely due to the distance and geometry (Figure S2). However, the hydroxyl group is in a plane with one of the water molecules complexing the Mg ion and the carboxyl groups of D107, E109, and E151. An interaction with the water molecule activated by the three acidic side chains or directly with E151 is sterically possible. Further insight into the catalysis might be derived by neutron scattering to reveal the protonation state of the active site, but even data from this method would not be explicit if both reactions occur simultaneously.

In the absence of PCP, it is not desirable to have a high reactivity because this would lead to hydrolysis of the acid anhydride bond. In this situation, the side chain of E109 is coordinated to the Mg ion and is replaced by a water molecule upon binding of PCP. This change in the coordination sphere of the Mg ion could potentially modulate the reactivity. However, since E109 is not conserved, such a modulation would not be a general mechanism. Thus far, the second Mg ion has not been described in structures of PPTs. Nevertheless, the environment of the water molecules found at the same position in the other structures indicates that the electron density might represent a Mg ion as well (Figures 3D–3F). A cation at this position would not only enhance the binding of CoA to Sfp but would also stabilize the additional negative charge of the 5′ phosphate after ppan transfer. Mutation of H90 to asparagine or alanine has a distinct, but not drastic, effect on the ppan transfer by Sfp (Mofid et al., 2004), although the mutation very likely disrupts the coordination of the second Mg ion and the 3′ phosphate of CoA. Therefore, it can be concluded that the second Mg ion is not essential for the catalysis or binding of CoA by the PPT.

The high structural similarity of the PCP/Sfp complex and the human ACP/PPT complex, together with sequential similarities in different PPTs, indicates that the mechanism of catalysis is conserved in group II PPTs from many organisms ranging from bacteria to mammals. The same is true for the recognition of the carrier protein by the PPT. The intermolecular hydrogen bond, the hydrophobic contacts between helix 2 of the carrier protein and the C-terminal domain of the PPT, and the glycine in the loop required for the proper connection of the two interactions sites are present in both structures.

The effect of certain residues of the PCP involved in a correct binding to Sfp was shown by site-directed mutagenesis. The breakup of the intermolecular hydrogen bond by substitution of the hydrogen-bond donor (Y36 of Sfp) with a proline leads to a drop in the affinity for PCP by a factor of >70 (K_D 0.74 versus 54.3 μM). The binding of Sfp(WT) to the PCP(G42A) mutant shows a similar drop in affinity, most likely due to a less favorable geometry for the formation of the intermolecular hydrogen bond, caused by a reorientation of the loop containing G42.

Remarkably, the reduced affinity does not lead to a slower conversion of the apo-PCPs. The velocities of the phosphopantetheinylation of TycC3_PCP(G42A) by Sfp(WT), and TycC3_PCP(WT) by Sfp(Y36P) are rather enhanced compared with the WT system. Although the presented data cannot explain this finding, one might speculate that the reduced affinity causes a faster dissociation of the holo-PCP/Sfp complex after the reaction, which enables the enzyme to undergo the next catalytic cycle faster. The conclusion that the hydrogen bond between the carrier protein and the PPT is not essential for the ppan transfer reaction is in agreement with results showing that also the small YbbR peptide (Figure 5E), mimicking only the second helix of a carrier protein, can be phosphopantetheinylated on its own or when fused to other proteins (Yin et al., 2005).

The structure of the PCP/Sfp complex suggests that the hydrophobic interaction between PCP's L46 and M49 located in this helix and a more extended nonpolar patch in Sfp's catalytic domain is the key element of their interaction, which is further supported by the mutational analysis. On the one hand, the slow modification of TycC3_PCP(L46N) and the hardly detectable formation of holo-TycC3_PCP(L46D) suggest that a

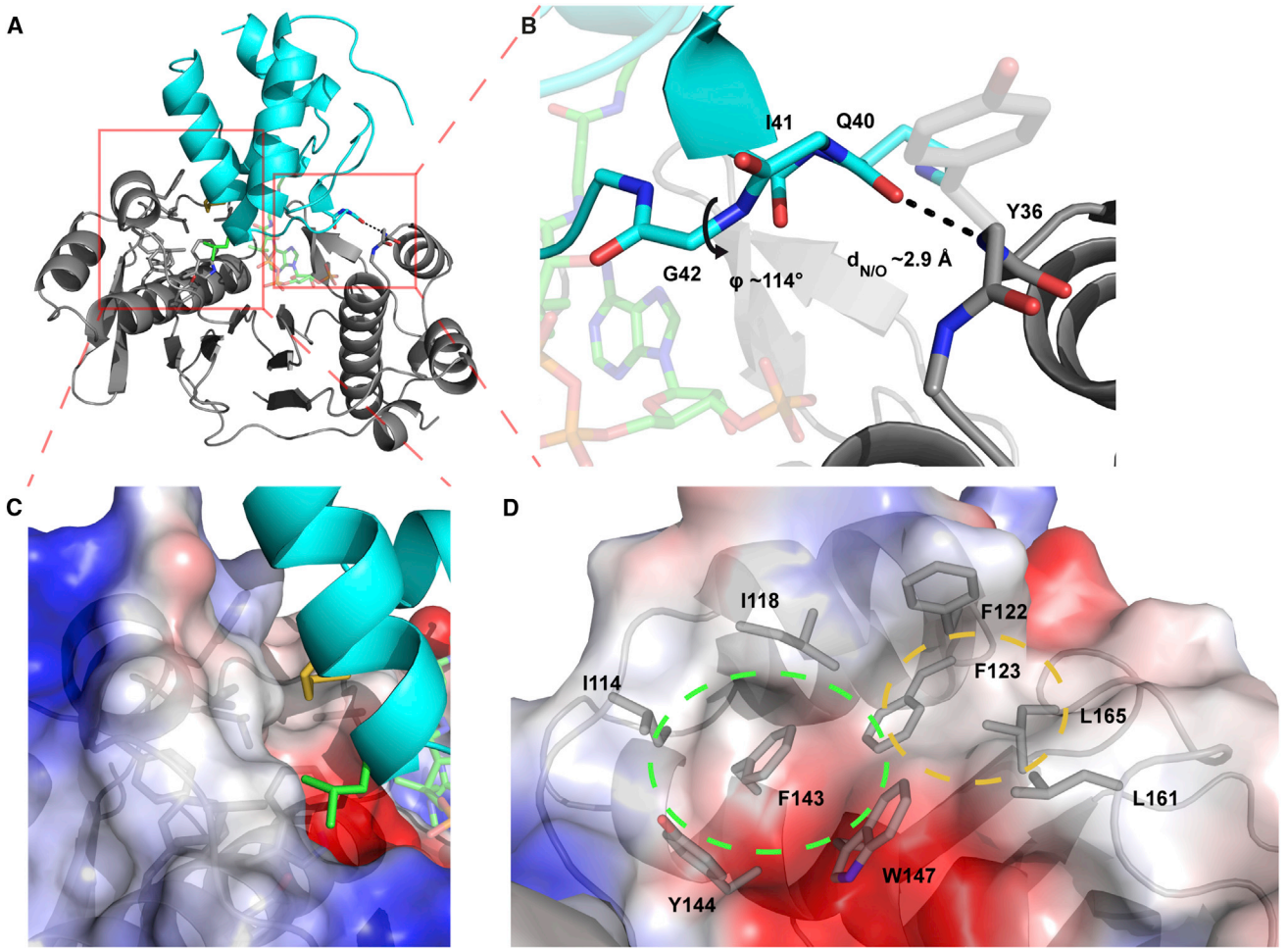

E

Group II PPTs

		β1	α1	α2	α3
Sfp	(104-165)	IGIDIEKTK-------PISLEIAKRFFSKTEYSDLL-AKDKDEQTDYFYHLWSMKESFIKQEGKGLSLPL			
EntD	(104-164)	IGIDIEEIFSVQT-----ARELTDNIITPAEHERLADCGLA--FSLALTLAFSAKESAFKAS--EIQTDA			
Lys5	(133-196)	VGIDIASPCNYGG---REELELFKEVFSEREFNGLLKASDP---CTIFTYLWSLKESYTKFTGTGLNTDL			
hPPT	(126-195)	VGIDIMKTSFPGRGSIPEFFHIMKRKFTNKEWETIRSFKDEWTQLDMFYRNWALKESFIKAIGVGLGFEL			

Carrier proteins (natural substrates to group II PPTs)

		helix 2
TycC	(31-59*)	GIGILDNFFQIGGHSLKAMAVAAQVHREY
EntB	(231-258)	EPFDDDNLIDYGLDSVRMMALAAR-WRKV
Lys2	(866-894)	SVSPDDSFFDLGGHSILATKMIFTLKKKL
hACP	(2137-2165)	AVNLGGSLADLGLDSLMSAPVRQTLEREL
		φ

Non-natural substrates to group II PPTs

		helix 2
AcpP	(23-51)	VTNNASFVEDLGADSLDTVELVMALEEEF
AcpA	(23-51)	VKLEASFKEDLGADSLDVVELVMELEDEF
ACP I	(80-108)	VVTADSEFSKLGADSLDTVEIVMNLEEEF
YbbR	(peptide)	----------DSLEFIASKLA-----
		φ

Figure 5. Protein-Protein Interactions in the Complex

(A) The binding of PCP (cyan) to Sfp (gray) is stabilized by hydrophobic interactions and an intermolecular hydrogen bond. The two interaction sites are linked by a loop harboring a conserved glycine.

(B) The hydrogen bond (dashed line) is formed by Q40 of the PCP and Y36 in the N-terminal domain of Sfp. G42 in the loop of the PCP has a positive φ torsion (arrow), which might be necessary for the correct orientation of the two interaction sites.

(C) The side chains of L46 (green sticks) and M49 (yellow sticks) in the second helix of the PCP point toward a hydrophobic patch in the C-terminal PPT domain (shown in electrostatic surface representation).

(D) A front view of this hydrophobic patch reveals a large cavity for binding of L46 (green circle) and a smaller one for M49 (yellow circle).

(legend continued on next page)

Table 1. Thermodynamic Data from the ITC Experiments

Sample	T (°C)	K_D (μM)	ΔH (kJ mol^{-1})	ΔS (J mol^{-1} K^{-1})	n
S45A + Sfp(WT)[a]	5	0.74 ± 0.04	15.6 ± 0.1	173.8	1.23 ± 0.01
S45A + Sfp(WT)[a]	25	0.92 ± 0.12	−10.7 ± 0.1	80.0	1.22 ± 0.01
S45A + Sfp(Y36P)[a]	5	54.3 ± 6.5	18.2 ± 2.3	147.0	1.00 ± 0.10
S45A + Sfp(Y36P)[a]	25	–	–	–	–
G42A/S45A + Sfp(WT)[a]	5[b]	39.7 ± 2.2	24.3 ± 1.2	171.7	1.08 ± 0.04
S45A/L46A + Sfp(WT)[a]	5/25	–	–	–	–
S45A/L46N + Sfp(WT)[a]	5/25	–	–	–	–
S45A/L46D + Sfp(WT)[a]	5/25	–	–	–	–
S45A/M49D + Sfp(WT)[a]	5/25	–	–	–	–
Sfp(WT) + CoA	5[b]	1.49 ± 0.17	−16.4 ± 0.3	52.3	0.78 ± 0.01
Sfp(Y36P) + CoA	5[b]	1.57 ± 0.18	−16.1 ± 0.2	53.2	1.10 ± 0.01

–, no apparent binding (K_D > 100 μM). See also Figure S3 and Table S1.
[a]3 mM CoA in buffer.
[b]Sample not stable at 25°C.

hydrophobic residue at this position is important. On the other hand, the L46A mutation has a significant effect as well, as its methyl group is too small to fill the binding pocket designed for a larger side chain. PCP's M49 does not point into such a well-defined binding pocket, which is why its substitution with an aspartate did not reduce the reaction velocity as strongly as the same substitution for L46, emphasizing the central role of PCP's L46 for the binding to Sfp. The PCP mutants harboring a mutation in helix 2 showed no detectable binding to Sfp(WT) in the ITC titration experiments. This indicates that a stronger reduction in affinity than was observed for either TycC3_PCP(WT)/Sfp(Y36P) or TycC3_PCP(G42A)/Sfp(WT) correlates with a slower reaction velocity. This correlation results in an almost complete abolishment of the modification of TycC3_PCP(L46N) when Sfp(WT) is substituted with Sfp(Y36P). For the reaction of TycC3_PCP(L46N) with Sfp(WT), the hydrophobic interactions are significantly disturbed by the L46N mutation, which leads to a slow reaction velocity. By an additional disruption of the intermolecular hydrogen bond, the apo-TycC3_PCP(L46N)/Sfp(Y36P) complex, formed prior to the reaction, is further destabilized and the reaction hardly occurs. Thus, the intermolecular hydrogen bond seems to play an important role in the modification of carrier proteins that would only bind very weakly to Sfp via their second helix. Furthermore, the hydrophobic character of the residues corresponding to L46 and M49 is conserved in many other carrier proteins involved in different metabolic pathways (Figure 5E), emphasizing the promiscuity of Sfp for diverse carrier proteins.

As carrier proteins are not only designed to be phosphopantetheinylated but are also involved in substrate shuttling, and in doing so act together with numerous other catalytic domains, it makes sense that only a few residues are crucial for each interdomain contact to retain the great variety of interactions.

SIGNIFICANCE

Sfp-like PPTs from pathogenic bacteria have been suggested as potential drug targets (Leblanc et al., 2012; Yasgar et al., 2010). The high similarity of the presented crystal structure of the PCP/Sfp complex to the structure of the human PPT/ACP complex suggests a potential problem in the development of such drugs. The comparable orientation of CoA and the carrier protein in the binding pockets of the two PPTs indicates that cofactor binding, substrate recognition, and the mechanism of the ppan transfer are highly conserved. Thus, a drug that inhibits a bacterial PPT by directly targeting its active site may have similar effects on the human PPT as well.

On the other hand, the similarities between the complexes of PCP/Sfp and the human PPT/ACP emphasize the applicability of group II PPTs in biotechnology. In principle, one could develop an enormous variety of substances by designing megasynthases that contain carrier proteins and other domains from NRPS, PKS, and FAS. Due to their high substrate tolerance with respect to the carrier protein, group II PPTs such as Sfp seem ideal for modifying the diverse ACPs and PCPs included in such artificial proteins. However, until now, most attempts to design productive megasynthases have not been very successful because the selectivity of the interactions of the other domains is not well understood and needs further investigation.

EXPERIMENTAL PROCEDURES

Cloning, Expression, and Purification of Sfp and PCP Variants

In this work, the previously described constructs of *sfp* in pQE60 (Mofid et al., 1999) and *tycC3_PCP* in pQE70 (Weber et al., 2000) were used. Mutants of

(E) Alignments of Sfp with other group II PPTs from *E. coli*, *Saccharomyces cerevisiae*, and *Homo sapiens*, and of TycC3_PCP (S45 in TycC3_PCP corresponds to S3075 in full-length TycC) with substrate carrier proteins of the PPTs, respectively, show that the properties of the side chains involved in cofactor binding (black) and protein-protein interaction (gray) are conserved. In addition, a glycine residue at the position of G42 of TycC3_PCP, which has a positive φ angle in the presented structures, is also conserved (indicated with a φ). Similar hydrophobic residues are also present in nonnatural substrates of Sfp, such as the ACPs of FAS from *E. coli*, *Bacillus subtilis*, and *Spinacia oleracea*, as well as in the small YbbR peptide.

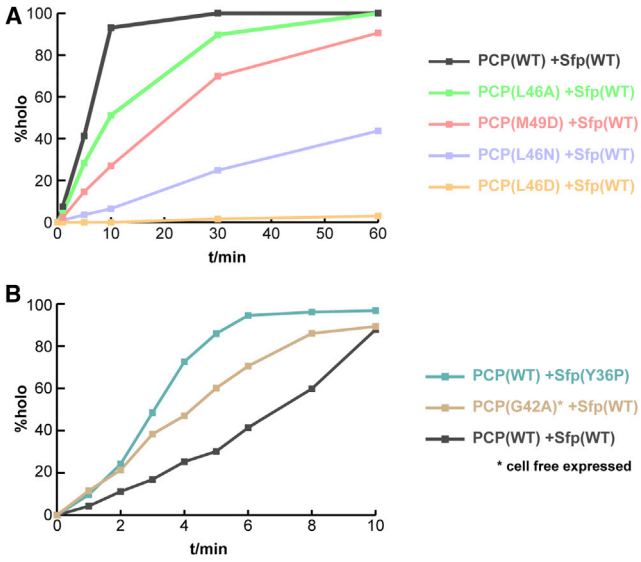

Figure 6. Reaction Velocities of the ppan Transfer

Mutations of residues involved in the hydrophobic interaction reduce the velocity of the ppan transfer (A), whereas disruption of the intermolecular hydrogen bond accelerates the reaction (B). A small portion of TycC3_PCP(G42A) precipitated during incubation, resulting in <100% product formation even after 1 hr (Figure S4A), and making it appear that holo-TycC3_PCP(G42A) formed more slowly than it actually does. For better clarity, error bars have been omitted because the SDs are rather small (i.e., max. 2.7% in A and 3.5% in B).

See also Figure S3 and Table S1.

both genes were cloned with PfuTurbo DNA polymerase (Agilent) (primers and procedures are described in Supplemental Experimental Procedures). All pQE plasmids were transformed into *Escherichia coli* M15(pREP4) cells (QIAGEN).

For expression of Sfp variants, 500 ml lysogeny broth (LB) medium supplemented with 100 μg/l ampicillin and 30 μg/l kanamycin was inoculated with 5 ml of an overnight culture, and grown at 37°C and 180 rpm. At an OD of 0.6, the temperature was lowered to 30°C and expression was induced by addition of isopropyl β-D-1-thiogalactopyranoside (IPTG) to a final concentration of 0.5 mM. After 4 hr, cells were harvested by centrifugation for 10 min at 6,000 rpm, resuspended in nickel buffer A (25 mM HEPES, 200 mM NaCl, 25 mM imidazole; pH 8.0), and lysed by ultrasonication. Proteins were purified by nickel affinity purification with a linear imidazole gradient (buffer B: 25 mM HEPES, 200 mM NaCl, 300 mM imidazole; pH 8.0), followed by dialysis and size-exclusion chromatography with a Superdex 75 column (GE Healthcare) in a suitable buffer.

Expression of nonlabeled PCP constructs was performed similarly at 20°C overnight, and the purification was done in the same way as described for Sfp. Isotopic-labeled samples were produced accordingly in M9 minimal medium supplemented with 1 g/l ^{15}N-ammonium chloride and 2 g/l ^{13}C-glucose.

Cell-free Expression and Purification of PCP Variants

Since the PCP variants harboring a glycine-to-alanine mutation showed no expression under several tested conditions, the genes were subcloned into the pBH4 vector (a pET15b variant with a cleavable N-terminal 6xHis tag). Again, no expression in vivo using *E. coli* BL21(DE3) cells (New England Biolabs) was observed, but the vector could be used for a T7 RNA polymerase-based transcription/translation cell-free expression system (Schwarz et al., 2007) to facilitate the production of insoluble proteins. These proteins were dissolved in 6 M urea and refolded by dialysis against 25 mM HEPES, 50 mM NaCl, 1 mM dithiothreitol (DTT), 0.5 mM EDTA (pH 7.2) at 4°C. The refolded proteins were treated with tobacco etch virus protease for 12–16 hr at 4°C and purified by reverse nickel affinity purification and subsequent dialysis and size-exclusion chromatography analogously to the in vivo expressed proteins.

As a control, TycC3_PCP(WT) and TycC3_PCP(S45A) were also subcloned into pBH4 and expressed cell free, resulting in insoluble proteins that were purified like the G42A mutants.

Crystallization, Data Collection, and Structure Determination of the PCP/Sfp Complex

TycC3_PCP(S45A) and Sfp(WT) were purified separately in 25 mM HEPES, 50 mM NaCl, 5 mM $MgCl_2$, and 5 mM DTT (pH 7.2), and mixed at a 1:1 molar ratio. CoA was added to the protein mixture to a final concentration of 1.5 mM. Final mixtures with monomer concentrations of 300, 500, and 750 μM were used for crystallization.

Diffraction-quality crystals were grown using the sitting-drop method by a Mosquito crystallization robot (TTP LabTech), with 0.16 M magnesium acetate, 0.08 M sodium cacodylate (pH 6.5), 16% (w/v) PEG 8000, and 20% (v/v) glycerol in the reservoir solution. The crystals formed overnight and were full grown within 3–4 days at 20°C. Preliminary diffraction data were collected to 2.6 Å resolution at the Max Planck Institute of Biophysics (Frankfurt, Germany) using the FR-E+ in-house diffractometer equipped with a Saturn 994+ CCD detector (Rigaku). The diffraction data were processed using HKL2000 (Evans, 2006). A preliminary structure of the complex was solved by employing the molecular replacement method using MOLREP from the CCP4 package (Winn et al., 2011), with the structure of the Sfp (PDB 1QR0) and the presented NMR structure as search models.

A data set of the crystals obtained by reproducing the previous conditions in hanging drops was collected at the PX3 beamline of the Swiss Light Source (Villigen, Switzerland). The diffraction data were processed using MOSFLM (Leslie and Powell, 2007) and the complex structure was determined by the molecular replacement method using the preliminary model obtained earlier from the data collected at the in-house diffractometer as a search model. The model was further built and refined using COOT (Emsley and Cowtan, 2004) and REFMAC5 (Murshudov et al., 2011), respectively. Data collection and refinement statistics are summarized in Table S2.

NMR Structure Determination

Resonance assignment of TycC3_PCP(S45A) was performed using triple-resonance spectra recorded at 298 K with a 700 μM uniformly [^{13}C; ^{15}N]-labeled protein sample in 50 mM sodium phosphate (NaP_i) buffer (pH 6.8) containing 5% D_2O and 0.15 mM 4,4-dimethyl-4-silapentane-1-sulfonate (DSS). All data were collected on Bruker Avance 600-950 MHz spectrometers equipped with triple-resonance cryo probes.

The completeness of the chemical-shift assignments for the nonlabile ^{1}H and the backbone H^N was 94%. 3D ^{15}N-resolved NOE spectroscopy/heteronuclear single-quantum coherence (NOESY-HSQC) and $^{13}C_{aromatic}$-resolved NOESY-HSQC spectra yielded peak lists from which NOE distance restraints were obtained by automatic NOESY cross-peak assignment and calibration using the program CYANA (Güntert, 2009; Herrmann et al., 2002) based on the chemical-shift lists (Table S3). Backbone dihedral angle restraints were created from chemical-shift data for the atoms H^N, N, C', C^α, C^β, and H^α using TALOS+ software (Shen et al., 2009).

The structure calculation was performed with CYANA using 100 random starting conformers and 10,000 torsion-angle dynamics steps. From the resulting structures, the 20 with the lowest target function values were selected. Restrained energy refinement was carried out using the OPALp program (Koradi et al., 2000).

Phosphopantetheinylation Assay

Proteins used in the phosphopantetheinylation assay were purified into 50 mM NaP_i (pH 6.8), 5 mM DTT, and 5 mM $MgCl_2$. The concentration of the PCP variants was adjusted to 105 μM and aliquots of 95 μl were made. The priming reaction, performed in triplicate, was started by adding 5 μl enzyme mix (10 μM Sfp/20 mM CoA) to each aliquot, and incubated at 25°C. The reaction was stopped with 100 μl precooled trichloroacetic acid (20% w/v) after the desired reaction time. The precipitates were pelleted by centrifugation for 30 min at 20,000 × *g* and 4°C, washed with 200 μl trichloroacetic acid followed by 200 μl diethyl ether, and dried in a centrifugal evaporator.

The dried pellets were dissolved in 50 μl aqueous trifluoroacetic acid (TFA; 0.1% v/v) and applied on a CC250/3 Nucleosil 120-3 C18 column (Macherey-Nagel) operated at 50°C. The separation of apo- and holo-PCPs was accomplished using a linear gradient from 45%–54.5% buffer B (45%–59% for the pBH4 constructs) over 27 min at a flow rate of 0.8 ml/min with 0.1% (v/v) TFA in water or acetonitrile as buffer A and buffer B, respectively. The different compounds were identified by electrospray ionization/mass spectrometry analysis with a detection range for m/z of 400–1,400, and quantified by their absorption at 214 nm measured in parallel.

Complex Stability Analysis

After purification, all PCP and Sfp variants were dialyzed against 50 mM NaP_i (pH 6.8) and 5 mM $MgCl_2$. Using a Slide-A-Lyzer dialysis cassette with a 3,500 Da cutoff (Thermo Scientific), a 100 mM CoA solution was subjected to the same dialysis.

For a first set of experiments, the proteins were diluted with dialysis buffer and supplemented with CoA and *tris*(2-carboxyethyl)phosphine (TCEP) to gain solutions with final concentrations of 50 μM PCP or 800 μM Sfp variant, 3 mM CoA and 2 mM TCEP. Active-site single- and double-mutant PCPs were injected into a VP-ITC calorimeter (MicroCal) and Sfp(WT) was titrated in 27 steps of 10 μl each, at both 5°C and 25°C. Sfp(Y36P) was titrated to the active-site mutant PCP in exactly the same manner.

For a second set of experiments, solutions of 50 μM Sfp (WT and Y36P) and 800 μM CoA, all with 2 mM TCEP, were prepared. CoA was titrated to both Sfp variants in 27 titration steps of 10 μl, but due to the reduced thermal stability of both Sfp variants in the absence of CoA, these experiments were only performed at 5°C.

ACCESSION NUMBERS

The atomic coordinates and structure factors of the PCP/Sfp complex structure, and the atomic coordinates and NMR restraints of TycC3_PCP(S45A) have been deposited in the Protein Data Bank under accession numbers 4MRT and 2MD9, respectively. The resonance assignment for the NMR structure can be found in the Biological Magnetic Resonance Bank under accession number 19479.

SUPPLEMENTAL INFORMATION

Supplemental Information includes Supplemental Experimental Procedures, four figures, and three tables and can be found with this article online at http://dx.doi.org/10.1016/j.chembiol.2014.02.014.

ACKNOWLEDGMENTS

We thank Laura Luh and Benedikt Kuhn for their support and helpful discussions during the development of this project. This work was supported by the Deutsche Forschungsgemeinschaft (DO545/7-1 and MA811/24-1), the Center for Biomolecular Magnetic Resonance (BMRZ), the Cluster of Excellence Frankfurt (Macromolecular Complexes), the Lichtenberg Program of the Volkswagen Foundation, and Instruct (part of the European Strategy Forum on Research Infrastructures [ESFRI]) and through national member agreements. S.R. was the recipient of an EMBO long-term fellowship.

Received: September 26, 2013
Revised: February 2, 2014
Accepted: February 6, 2014
Published: April 3, 2014

REFERENCES

Beld, J., Sonnenschein, E.C., Vickery, C.R., Noel, J.P., and Burkart, M.D. (2014). The phosphopantetheinyl transferases: catalysis of a post-translational modification crucial for life. Nat. Prod. Rep. *31*, 61–108.

Belshaw, P.J., Walsh, C.T., and Stachelhaus, T. (1999). Aminoacyl-CoAs as probes of condensation domain selectivity in nonribosomal peptide synthesis. Science *284*, 486–489.

Bunkoczi, G., Pasta, S., Joshi, A., Wu, X., Kavanagh, K.L., Smith, S., and Oppermann, U. (2007). Mechanism and substrate recognition of human holo ACP synthase. Chem. Biol. *14*, 1243–1253.

Chan, D.I., and Vogel, H.J. (2010). Current understanding of fatty acid biosynthesis and the acyl carrier protein. Biochem. J. *430*, 1–19.

Condurso, H.L., and Bruner, S.D. (2012). Structure and noncanonical chemistry of nonribosomal peptide biosynthetic machinery. Nat. Prod. Rep. *29*, 1099–1110.

Crosby, J., and Crump, M.P. (2012). The structural role of the carrier protein—active controller or passive carrier. Nat. Prod. Rep. *29*, 1111–1137.

Ehmann, D.E., Gehring, A.M., and Walsh, C.T. (1999). Lysine biosynthesis in Saccharomyces cerevisiae: mechanism of alpha-aminoadipate reductase (Lys2) involves posttranslational phosphopantetheinylation by Lys5. Biochemistry *38*, 6171–6177.

Elovson, J., and Vagelos, P.R. (1968). Acyl carrier protein. X. Acyl carrier protein synthetase. J. Biol. Chem. *243*, 3603–3611.

Emsley, P., and Cowtan, K. (2004). Coot: model-building tools for molecular graphics. Acta Crystallogr. D Biol. Crystallogr. *60*, 2126–2132.

Evans, P. (2006). Scaling and assessment of data quality. Acta Crystallogr. D Biol. Crystallogr. *62*, 72–82.

Fichtlscherer, F., Wellein, C., Mittag, M., and Schweizer, E. (2000). A novel function of yeast fatty acid synthase. Subunit alpha is capable of self-pantetheinylation. Eur. J. Biochem. *267*, 2666–2671.

Güntert, P. (2009). Automated structure determination from NMR spectra. Eur. Biophys. J. *38*, 129–143.

Herrmann, T., Güntert, P., and Wüthrich, K. (2002). Protein NMR structure determination with automated NOE assignment using the new software CANDID and the torsion angle dynamics algorithm DYANA. J. Mol. Biol. *319*, 209–227.

Hur, G.H., Vickery, C.R., and Burkart, M.D. (2012). Explorations of catalytic domains in non-ribosomal peptide synthetase enzymology. Nat. Prod. Rep. *29*, 1074–1098.

Johansson, P., Mulinacci, B., Koestler, C., Vollrath, R., Oesterhelt, D., and Grininger, M. (2009). Multimeric options for the auto-activation of the Saccharomyces cerevisiae FAS type I megasynthase. Structure *17*, 1063–1074.

Keatinge-Clay, A.T. (2012). The structures of type I polyketide synthases. Nat. Prod. Rep. *29*, 1050–1073.

Koglin, A., Mofid, M.R., Löhr, F., Schäfer, B., Rogov, V.V., Blum, M.M., Mittag, T., Marahiel, M.A., Bernhard, F., and Dötsch, V. (2006). Conformational switches modulate protein interactions in peptide antibiotic synthetases. Science *312*, 273–276.

Koradi, R., Billeter, M., and Güntert, P. (2000). Point-centered domain decomposition for parallel molecular dynamics simulation. Comput. Phys. Commun. *124*, 139–147.

Kosa, N.M., Haushalter, R.W., Smith, A.R., and Burkart, M.D. (2012). Reversible labeling of native and fusion-protein motifs. Nat. Methods *9*, 981–984.

La Clair, J.J., Foley, T.L., Schegg, T.R., Regan, C.M., and Burkart, M.D. (2004). Manipulation of carrier proteins in antibiotic biosynthesis. Chem. Biol. *11*, 195–201.

Lambalot, R.H., Gehring, A.M., Flugel, R.S., Zuber, P., LaCelle, M., Marahiel, M.A., Reid, R., Khosla, C., and Walsh, C.T. (1996). A new enzyme superfamily—the phosphopantetheinyl transferases. Chem. Biol. *3*, 923–936.

Leblanc, C., Prudhomme, T., Tabouret, G., Ray, A., Burbaud, S., Cabantous, S., Mourey, L., Guilhot, C., and Chalut, C. (2012). 4′-Phosphopantetheinyl transferase PptT, a new drug target required for Mycobacterium tuberculosis growth and persistence in vivo. PLoS Pathog. *8*, e1003097.

Leslie, A.W., and Powell, H. (2007). Processing diffraction data with mosflm. In Evolving Methods for Macromolecular Crystallography, R. Read and J. Sussman, eds. (Dordrecht, The Netherlands: Springer), pp. 41–51.

Liu, Y., and Bruner, S.D. (2007). Rational manipulation of carrier-domain geometry in nonribosomal peptide synthetases. ChemBioChem *8*, 617–621.

Lomakin, I.B., Xiong, Y., and Steitz, T.A. (2007). The crystal structure of yeast fatty acid synthase, a cellular machine with eight active sites working together. Cell *129*, 319–332.

Mofid, M.R., Marahiel, M.A., Ficner, R., and Reuter, K. (1999). Crystallization and preliminary crystallographic studies of Sfp: a phosphopantetheinyl transferase of modular peptide synthetases. Acta Crystallogr. D Biol. Crystallogr. *55*, 1098–1100.

Mofid, M.R., Finking, R., Essen, L.O., and Marahiel, M.A. (2004). Structure-based mutational analysis of the 4′-phosphopantetheinyl transferases Sfp from Bacillus subtilis: carrier protein recognition and reaction mechanism. Biochemistry *43*, 4128–4136.

Murshudov, G.N., Skubák, P., Lebedev, A.A., Pannu, N.S., Steiner, R.A., Nicholls, R.A., Winn, M.D., Long, F., and Vagin, A.A. (2011). REFMAC5 for the refinement of macromolecular crystal structures. Acta Crystallogr. D Biol. Crystallogr. *67*, 355–367.

Parris, K.D., Lin, L., Tam, A., Mathew, R., Hixon, J., Stahl, M., Fritz, C.C., Seehra, J., and Somers, W.S. (2000). Crystal structures of substrate binding to Bacillus subtilis holo-(acyl carrier protein) synthase reveal a novel trimeric arrangement of molecules resulting in three active sites. Structure *8*, 883–895.

Praphanphoj, V., Sacksteder, K.A., Gould, S.J., Thomas, G.H., and Geraghty, M.T. (2001). Identification of the alpha-aminoadipic semialdehyde dehydrogenase-phosphopantetheinyl transferase gene, the human ortholog of the yeast LYS5 gene. Mol. Genet. Metab. *72*, 336–342.

Reuter, K., Mofid, M.R., Marahiel, M.A., and Ficner, R. (1999). Crystal structure of the surfactin synthetase-activating enzyme sfp: a prototype of the 4′-phosphopantetheinyl transferase superfamily. EMBO J. *18*, 6823–6831.

Schwarz, D., Junge, F., Durst, F., Frölich, N., Schneider, B., Reckel, S., Sobhanifar, S., Dötsch, V., and Bernhard, F. (2007). Preparative scale expression of membrane proteins in Escherichia coli-based continuous exchange cell-free systems. Nat. Protoc. *2*, 2945–2957.

Shen, Y., Delaglio, F., Cornilescu, G., and Bax, A. (2009). TALOS+: a hybrid method for predicting protein backbone torsion angles from NMR chemical shifts. J. Biomol. NMR *44*, 213–223.

Sieber, S.A., Walsh, C.T., and Marahiel, M.A. (2003). Loading peptidyl-coenzyme A onto peptidyl carrier proteins: a novel approach in characterizing macrocyclization by thioesterase domains. J. Am. Chem. Soc. *125*, 10862–10866.

Weber, T., Baumgartner, R., Renner, C., Marahiel, M.A., and Holak, T.A. (2000). Solution structure of PCP, a prototype for the peptidyl carrier domains of modular peptide synthetases. Structure *8*, 407–418.

Winn, M.D., Ballard, C.C., Cowtan, K.D., Dodson, E.J., Emsley, P., Evans, P.R., Keegan, R.M., Krissinel, E.B., Leslie, A.G., McCoy, A., et al. (2011). Overview of the CCP4 suite and current developments. Acta Crystallogr. D Biol. Crystallogr. *67*, 235–242.

Worthington, A.S., and Burkart, M.D. (2006). One-pot chemo-enzymatic synthesis of reporter-modified proteins. Org. Biomol. Chem. *4*, 44–46.

Yasgar, A., Foley, T.L., Jadhav, A., Inglese, J., Burkart, M.D., and Simeonov, A. (2010). A strategy to discover inhibitors of Bacillus subtilis surfactin-type phosphopantetheinyl transferase. Mol. Biosyst. *6*, 365–375.

Yin, J., Straight, P.D., McLoughlin, S.M., Zhou, Z., Lin, A.J., Golan, D.E., Kelleher, N.L., Kolter, R., and Walsh, C.T. (2005). Genetically encoded short peptide tag for versatile protein labeling by Sfp phosphopantetheinyl transferase. Proc. Natl. Acad. Sci. USA *102*, 15815–15820.

